Anatomy-Guided Multimodal Graph Networks for Alzheimer's Disease: Integrative Analysis of Cross-Modal Brain Connectivity Signatures

Wenzheng Hu[1,2], Zhenghua Guan[1,2], Peng Yang[1,2], Jiaqiang Li[1,2],Yi Liu[1,2],Shushen Gan[1],Tuo Cai[1,2],Ao Zhang[1,2],Tengda Zhang[1,2],Junlong Qu[1,2],Shaolong Wang[1,2,],Gege Cai[1,2],Xiang Dong[1,2,],Tianfu Wang[1,2,⋆],Baiying Lei[1,2,⋆]

[1] School of Biomedical Engineering, Shenzhen University Medical School, Shenzhen University.
[2] Guangdong Key Laboratory for Biomedical Measurements and Ultrasound Imaging, National-Regional Key Technology Engineering Laboratory for Medical Ultrasound.

Abstract. Multimodal neuroimaging grounded in standardized brain atlases enables precise decoding of Alzheimer's progression by capturing both structural atrophy and functional decline across neural circuits. Current methods compromise anatomical fidelity in whole-brain modeling while generating biologically inconsistent cross-modal interactions. To address these dual challenges, we develop a graph learning framework that integrates three synergistic components: anatomically constrained feature extraction preserving region-specific biomarkers through spatial priors, channel-wise attention mechanisms for discriminative pattern refinement, and bidirectional cross-modal adaptation governed by alternating attention to enforce neuropathological consistency. This unified architecture processes sMRI and PET data through sequential stages of anatomical feature preservation, noise-robust feature enhancement, and dynamic modality fusion, ultimately mapping neurodegeneration patterns across scales. Evaluated on ADNI, our framework achieves superior classification accuracy while graph topology analysis reveals clinically significant hub reorganization within the default mode network, directly correlating with progressive connectivity deterioration. The method's capacity to reconcile localized biomarker specificity with systemic network dynamics establishes new standards for computational neuropathology.

Keywords: Alzheimer's disease · Graph Neural Networks · Anatomy Guided Learning · Brain Network Analysis · Multimodal Graph Learning.

1 Introduction

Alzheimer's disease (AD) is a neurodegenerative disorder characterized by progressive structural degradation, such as cortical thinning and white matter rarefaction, leading to widespread functional and structural impairments within

⋆ ✉Corresponding authors: Tianfu Wang (Email: tfwang@szu.edu.cn), and Baiying Lei (Email: leiby@szu.edu.cn)

interconnected neural networks [1][2]. AD pathogenesis is not confined to specific regions but affects multifocal brain areas, disrupting their functional and structural integrity [3][27]. Understanding how these changes manifest across anatomical structures is crucial, with brain imaging offering a valuable window into the spatiotemporal progression of neurodegeneration [8][23][24]. Crucially, AD follows axonal connectivity patterns rather than anatomical boundaries, highlighting the need for neuroimaging approaches that capture functional reconfiguration and the evolution of brain network dynamics over time [28][26].

Analyzing brain region features for AD progression faces several challenges: (1) capturing pathological changes while preserving spatial structure, such as distinguishing hippocampal atrophy from nearby areas [8]; (2) modeling complex spatial and functional dependencies among regions [9]; and (3) integrating multimodal data like sMRI and PET, which vary in resolution, signal type, and scale [10]. High-dimensional features also risk redundancy and overfitting, requiring mechanisms to enhance relevance and interpretability. Graph-based models (e.g., BrainMAE [7]) capture inter-regional relations and are commonly used for functional connectivity, though recent studies have extended them to structural and morphometric similarity networks as well, region-based methods (e.g., Zuo et al. These limitations point to the need for approaches that retain detailed structure while modeling inter-regional relationships. These limitations point to the need for approaches that retain detailed structure while modeling inter-regional relationships. To this end, we propose a multimodal graph learning framework with three components: (1) anatomy-guided feature extraction from sMRI and PET to capture clinical biomarkers; (2) channel-wise feature enhancement to emphasize discriminative patterns; and (3) dynamic cross-modal fusion to integrate complementary features and reorganize inter-region representations.

This tripartite architecture integrates spatial, structural, and functional insights to enhance AD classification and progression modeling. Evaluated on the ADNI cohort, our framework achieves superior diagnostic accuracy through anatomically constrained multimodal fusion. Comparative and ablation studies demonstrate biologically plausible feature integration with enhanced stability via adaptive modality synergy. Graph topology analysis reveals neurodegenerative mechanisms through memory-critical hub reorganization in hippocampal-entorhinal and olfactory pathways, uncovering the transition from localized compensation to global network collapse directly linked to clinical memory decline.

Our primary contributions can be summarized as follows:

- **Anatomy-guided Feature Extraction:** Utilizes clinically validated brain parcellation atlases for extracting region-specific biomarkers, such as hippocampal volume and amyloid burden derived from amyloid-PET imaging..
- **Channel-wise Feature Enhancement:** Implements a module to refine important features at the channel level, reducing irrelevant noise and improving model interpretability.
- **Dynamic Cross-modal Fusion:** Introduces the Cross-Graph Co-Attention (CGCA) mechanism to adaptively combine structural sMRI and PET data, enhancing the representation of neurodegeneration stages.

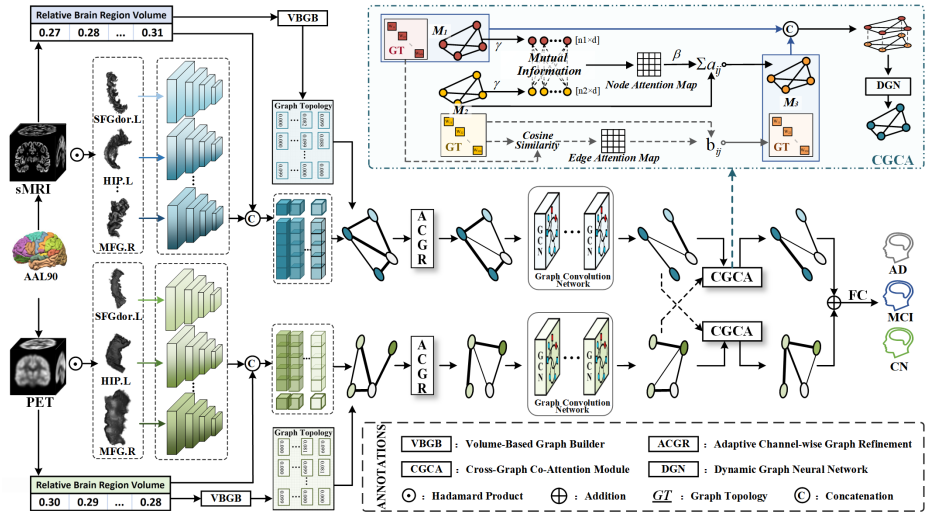

Fig. 1. Overview of our framework, integrating sMRI and PET via graph-based feature extraction and cross-modal co-attention for AD classification.

2 Methodology

2.1 Preliminaries

Graph convolutional networks (GCNs)[12] update node features by aggregating information from connected neighbors, a process mathematically expressed through neighborhood propagation rules. In a typical graph convolutional framework, node features $\mathbf{x}$ are updated via neighborhood aggregation using an adjacency matrix $\mathbf{A}$ and a degree matrix $\mathbf{D}$. Capturing interactions between brain regions is essential for understanding network-level disruptions in AD.To capture disease-relevant covariation patterns reflecting synchronized degeneration across brain regions, our Volume-Based Graph Builder (VBGB) quantifies structural covariance directly from imaging data using relative volume similarity. For each combination of imaging modality $m \in \{\text{sMRI}, \text{PET}\}$ and diagnostic contrast group $c \in \{\text{AD vs. CN}, \text{AD vs. MCI}, \text{MCI vs. CN}\}$, We compute pairwise Euclidean distances between $N = 90$ brain regions' normalized volume vectors $\mathbf{v}_i^{(m,c)}$, defined as below.The adjacency matrix $\mathbf{A}^{(m,c)} \in \{0,1\}^{N\times N}$ is then sparsified via k-nearest neighbors (k-NN)[13].

$$\mathbf{B}_{ij}^{(m,c)} = \left\|\mathbf{v}_i^{(m,c)} - \mathbf{v}_j^{(m,c)}\right\|_2^2, \quad \mathbf{A}_{ij}^{(m,c)} = \begin{cases} 1, & \text{if } j \in \text{TopK}(\mathbf{D}_i^{(m,c)}, k), \\ 0, & \text{otherwise.} \end{cases} \tag{1}$$

where closer Euclidean distances indicate stronger volumetric covariation. This generates six distinct graphs $\{\mathbf{G}^{(m,c)}\}$, encoding modality and disease stage-specific structural covariance patterns critical for early network-level pathology detection.

Overview of Our Method: To overcome the anatomical distortions in traditional multimodal fusion, this study constructs an anatomically constrained graph neural network framework. Using the AAL atlas[14], sMRI and PET data are precisely mapped to 90 functional brain regions, while a lightweight 3D CNN[15] extracts regional features . To eliminate individual differences, relative volume correction is introduced. An anatomy-driven sparse graph construction strategy retains only region-to-region associations consistent with structural covariance patterns, effectively reducing non-physiological connection noise. The core innovation lies in a dynamic fusion mechanism within anatomical units—the CGCA module, which, based on AD pathology stages, calculates mutual information between sMRI/PET nodes within specific functional systems and dynamically adjusts cross-modal weights, thereby enhancing multimodal feature integration in key regions such as the hippocampus and entorhinal cortex.

2.2 Anatomical Brain Region Recoding

Anatomical Brain Region$_{enc}$: To link neuroimaging data with region-specific biomarkers for brain disorders, we develop a feature-encoding framework that ensures anatomical consistency across subjects. Our pipeline applies affine registration, intensity normalization, and region extraction using a standardized atlas. Each brain region is zero-padded, spatially normalized, and reshaped into a uniform 3D representation.We extract isotropic 32^3 voxel blocks from 90 cortical and subcortical regions in the AAL[14] atlas. To reduce boundary artifacts, mirror padding is applied. The extracted regions are processed by a lightweight 3D-CNN [15] to encode morphological and metabolic differences. We further compute absolute volume v_i^{abs} and relative volume $v_i^{\text{rel}} = v_i / \left(\sum_{j=1}^{90} v_j + \epsilon\right)$, to model inter-regional volumetric relationships. The fused feature vector $\mathbf{x}_i \in \mathbb{R}^{514}$ captures both local tissue properties and global structural patterns , providing a neuroanatomically informed basis for disease characterization.

2.3 Anatomy-Aware Graph Learning Framework

Adaptive Channel-wise Graph Refinement: After building brain region graphs, we develop a dynamic graph refinement method(shown in Fig.2). Traditional approaches using fixed or random connections often miss complex inter-region relationships[12]. Our method combines actual anatomical connections with learnable weights, maintaining structural plausibility . The key component is a learnable shared topology $\mathbf{T} \in \mathbb{R}^{N \times N}$, constructed based on brain region volume ratios to dynamically optimize the connectivity graph. Unlike conventional methods that randomly generate connections, we incorporate anatomical priors to impose biologically meaningful connectivity patterns. The refinement employs two complementary functions : $\mathbf{F_1}$ models channel-wise relationships , while $\mathbf{F_2}$ enhances feature distinctiveness by extracting discriminative patterns.

$$\mathbf{F_1}(x_i, x_j) = \alpha(\lambda \cdot \tanh(\varphi_1(x_i) - \varphi_2(x_j))) \otimes \mathbf{T} \tag{2}$$

$$\mathbf{F_2}(x_i, x_j) = \text{MLP}(\varphi_1(x_i) \oplus \varphi_2(x_j)) \tag{3}$$

We use two dimension reducers (φ_1, φ_2) to reduce computational complexity. Learnable weights $\alpha \in \mathbb{R}^C$ adjust channel importance, while λ enhances feature contrasts through linear transformations. The fused topology is formulated as $\mathbf{M}' = (\alpha \otimes \mathbf{M}) \times \mathbf{T}$ where α scales channels, and $\mathbf{T}$ enforces anatomical constraints. Each channel's features are refined via $\sum_{j=1}^{m'} \beta(m_i \oplus x_i)$ and then aggregated into the final output. This adaptive convolution dynamically refines graphs per sample while preserving brain structural integrity, outperforming fixed methods in both accuracy and efficiency.

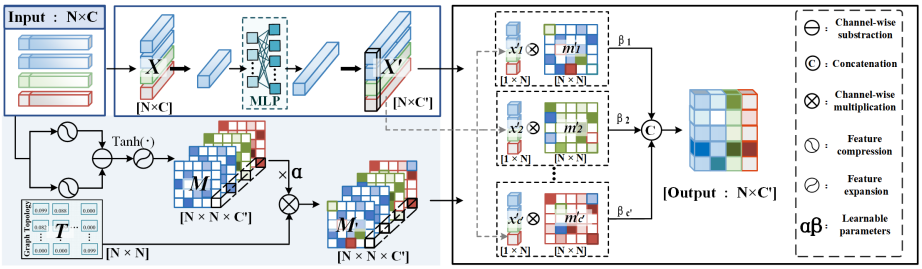

Fig. 2. ACGR: A dynamic brain network model integrating anatomical priors and task-specific functions through dual-path graph generation and fusion.

Cross-graph co-attention process: Existing multimodal fusion methods often overlook anatomical constraints, leading to biologically implausible feature mixing. Since brain regions are fundamental functional units, preserving their spatial relationships is essential. To address this, the CGCA module jointly refines node features and graph topology through dual-path collaborative learning, as detailed in Algorithm 1. Given a primary modality $\mathbf{M_1}$ (with n_1 nodes and d-dimensional features) and an auxiliary modality $\mathbf{M_2}$ (with n_2 nodes and d-dimensional features), we first establish cross-modal associations via:

$$e_{ij} = \beta \cdot -\mathbf{MI}(n_i^{\mathbf{M_1}}, n_j^{\mathbf{M_2}}), \quad e' = \beta \cdot \frac{\langle \mathbf{G_1}, \mathbf{G_2} \rangle}{\|\mathbf{G_1}\|_{F_1} \|\mathbf{G_2}\|_{F_2}} \tag{4}$$

where $\mathbf{MI}(\cdot)$ quantifies mutual information, and $\mathbf{G_1}, \mathbf{G_2} \in \mathbb{R}^{90\times 90}$ are topology matrices encoding structural embeddings. Attention weights are assigned as:

$$a_{ij} = \frac{\exp(e_{ij})}{\sum_{k=1}^{n_2} \exp(e_{ik})}, \quad b_{ij} = e' \tag{5}$$

Since cosine similarity is inherently normalized, b_{ij} propagates topological relationships, enabling simultaneous feature aggregation and topology refinement:

$$n_i^{M_3} = \sum_{j=1}^{n_2} a_{ij} n_j^{M_2}, \quad \mathbf{G_3} = b_{ij} \times \mathbf{G_{M_2}} \tag{6}$$

The fused modality $\mathbf{M_3}$ integrates the updated features as $\mathbf{M_3} = [n^{\mathbf{M_1}} \oplus n^{\mathbf{M_2}}]$, which is then processed by a dynamic GNN [16] with learnable adjacency matrices. Bidirectional fusion further refines representations by swapping $\mathbf{M_1}/\mathbf{M_2}$

roles, yielding enhanced feature-topology pairs $\{F^{\mathbf{M_1}}, A^{\mathbf{M_1}}_{\text{new}}\}$ and $\{F^{\mathbf{M_2}}, A^{\mathbf{M_2}}_{\text{new}}\}$. CGCA's co-optimization of features and topology effectively mitigates semantic-structural misalignment in cross-modal medical imaging analysis.

Algorithm 1 CGCA Fusion Process

Input: M_1: $\mathbf{N}_1 \in \mathbb{R}^{90\times256}$, $\mathbf{A}_1 \in \mathbb{R}^{90\times90}$; M_2: $\mathbf{N}_2 \in \mathbb{R}^{90\times256}$, $\mathbf{A}_2 \in \mathbb{R}^{90\times90}$
Output: M_{out}: $\mathbf{N}_{\text{out}} \in \mathbb{R}^{90\times256}$, $\mathbf{A}_{\text{out}} \in \mathbb{R}^{90\times90}$
Stage 1: Cross-modal Correlation Learning
for $i = 1$ **to** 90 **do**
  for $j = 1$ **to** 90 **do**
    Node correlation: $e_{ij} \leftarrow \beta \cdot \exp(-MI(\mathbf{N}_1[i], \mathbf{N}_2[j]))$
    Edge correlation: $e'_{ij} \leftarrow \beta \cdot \cos(\mathbf{A}_1[i], \mathbf{A}_2[j])$
  end for
  Node attention: $\mathbf{a}_i \leftarrow \text{Softmax}([e_{i1}, ..., e_{i90}])$
  Edge attention: $\mathbf{b}_i \leftarrow \text{Softmax}([e'_{i1}, ..., e'_{i90}])$
end for
Stage 2: Intermediate Modality Generation
for $i = 1$ **to** 90 **do** $\mathbf{v}_i \leftarrow \sum_{j=1}^{90} a_{ij} \cdot \mathbf{N}_2[j]$
end for
Stage 3: Modality Aggregation
$\mathbf{A}_{\text{new}} \leftarrow \mathbf{A}_1 \odot \mathbf{B}$ $\mathbf{N}_{\text{mid}} \leftarrow [\mathbf{v}_1^\top; ...; \mathbf{v}_{90}^\top]^\top$
$\mathbf{N}_{\text{out}} \leftarrow \text{MLP}([\mathbf{N}_1 \oplus \mathbf{N}_{\text{mid}}])$ $\mathbf{A}_{\text{out}} \leftarrow \text{DGCN}(\mathbf{A}_{\text{new}}, \mathbf{N}_{\text{out}})$ **return** $\mathbf{N}_{\text{out}}, \mathbf{A}_{\text{out}}$

3 Experiments

In our study, the ADNI dataset was utilised, which comprised 1,114 subjects across three diagnostic groups: 290 AD, 506 MCI, and 318 NC. The dataset under consideration encompasses sMRI and amyloid PET data. sMRI data underwent preprocessing using SPM12 and CAT12, a process that entailed steps such as denoising, bias correction, spatial normalisation, and grey matter segmentation. The data were then separated into two sets: a training set and a test set (in a ratio of 8:2). This was achieved using a fixed random seed, with subject ID-based partitioning in order to prevent data leakage.

3.1 Comparative Experiment

Current neuroimaging methods for AD often suffer from anatomically implausible cross-modality fusion, undermining biological plausibility. Patch-based approaches[5] mechanically combine MRI/PET features from arbitrary image partitions, leading to non-anatomical mixing. Global methods avoid this by reducing regions to scalar metrics but lose spatial granularity. Our anatomy-guided fusion resolves both issues by aligning sMRI/PET features within anatomical boundaries, enabling meaningful cross-modal interactions and enhancing hippocampal-entorhinal specificity. Moreover, our dynamic weighting mechanism adaptively captures AD-specific multimodal disruptions while reducing performance variability. These findings support a core hypothesis: fusion should respect neuroanatomical structure rather than rely on biologically agnostic feature aggregation.

Table 1. Performance Comparison for Classification Tasks.

Method	AD vs. CN			MCI vs. CN			AD vs. MCI		
	ACC(%)	AUC(%)	F1(%)	ACC(%)	AUC(%)	F1(%)	ACC(%)	AUC(%)	F1(%)
ResNet3D[17]	90.46±3.12	94.68±0.29	91.72±3.00	69.47±1.32	73.31±3.77	60.69±9.58	79.85±3.42	85.36±4.01	84.82±2.77
Att3D[18]	87.70±3.04	91.38±3.41	88.08±2.74	69.17±3.80	69.83±2.72	64.02±2.04	78.15±2.54	83.23±2.94	83.34±2.54
Senet[19]	88.92±3.64	92.53±3.50	88.71±3.55	70.72±1.92	69.00±4.87	60.27±9.37	80.48±2.09	86.52±3.15	85.10±1.81
BrainBagNet[5]	83.80±2.84	91.13±2.16	85.24±1.86	67.67±3.92	69.88±6.35	59.04±5.43	76.99±3.55	81.51±3.54	82.62±2.98
Zuo et al.[6]	89.16±2.71	93.23±1.93	85.09±5.41	69.46±2.99	66.66±5.76	64.92±6.94	78.48±1.41	82.92±3.71	83.42±1.96
BrainMAE[7]	91.56±2.94	94.71±1.94	84.47±8.07	70.45±2.92	73.33±4.58	63.46±2.94	79.85±3.42	85.36±4.01	84.82±2.77
Ours	**95.23±2.25**	**97.77±1.53**	**95.48±2.12**	**74.65**±5.35	**76.93**±6.53	**65.68**±8.58	**83.29**±2.38	**88.58**±1.57	**87.16**±1.73

3.2 Ablation Study

Progressive Module Validation: The baseline model showed limited performance in classification. Incorporating anatomical constraints(ABRE) significantly improved AD classification and enhanced MCI classification stability.Further introducing dynamic graph refinement(ACGR) boosted ADvs.MCI differentiation but introduced fluctuations in early MCI detection.The optimal configuration(ABRE+CGCA) achieved the highest stability in AD classification, while the full model leveraged cross-modal synergy for comprehensive optimization.
Multimodal Synergy. sMRI performed best in AD detection, whereas PET excelled in early MCI identification. Dual-modal fusion significantly enhanced classification performance, achieving peak AD detection while reducing cross-modal noise interference.However, increased variance in MCI classification suggests the need for adaptive fusion strategies to address early-stage heterogeneity.

Table 2. Validating Model Components: Ablation Study

Module			AD vs. CN		MCI vs. CN		AD vs. MCI	
ABRE	ACGR	CGCA	ACC	AUC	ACC	AUC	ACC	AUC
			88.31±4.10	88.38±5.22	67.68±2.98	69.72±5.38	79.85±2.36	84.74±3.65
✓			89.22±4.18	93.24±3.56	68.97±3.49	70.96±4.67	80.99±2.15	84.23±4.06
✓	✓		90.18±3.23	94.20±2.10	69.50±3.47	70.34±6.24	80.92±2.63	86.56±3.47
✓		✓	93.69±1.97	96.25±1.84	71.66±2.45	73.35±4.65	81.53±2.93	86.73±3.08
✓	✓	✓	95.23±2.25	97.77±1.53	74.65±5.35	76.93±6.53	83.29±2.38	88.58±1.57
	Modality		AD vs. CN		MCI vs. CN		AD vs. MCI	
	sMRI	PET	ACC	AUC	ACC	AUC	ACC	AUC
	✓		91.57±3.91	95.18±3.75	71.22±2.36	72.70±4.41	81.11±2.59	86.42±3.80
		✓	92.25±2.22	94.82±2.53	72.50±2.78	74.51±4.80	81.42±3.87	83.15±4.56
	✓	✓	95.23±2.25	97.77±1.53	74.65±5.35	76.93±6.53	83.29±2.38	88.58±1.57

3.3 Brain Network Analysis

Brain network analysis: Our graph-based topology analysis reveals significant rewiring of brain networks during AD progression. Stronger EC-HIP connectivity in MCI is linked to preserved episodic memory but also predicts faster cognitive decline, suggesting a trade-off between local compensation and global pathology spread. Centrality analysis identifies the OLF-EC pathway as a key hub, whose

disruption sharply reduces network efficiency, marking a critical transition in disease progression. By integrating sMRI and PET features via our anatomy-guided GNN , we enhance MCI-to-AD conversion prediction over unimodal models, with topological metrics explaining a significant portion of clinical decline.

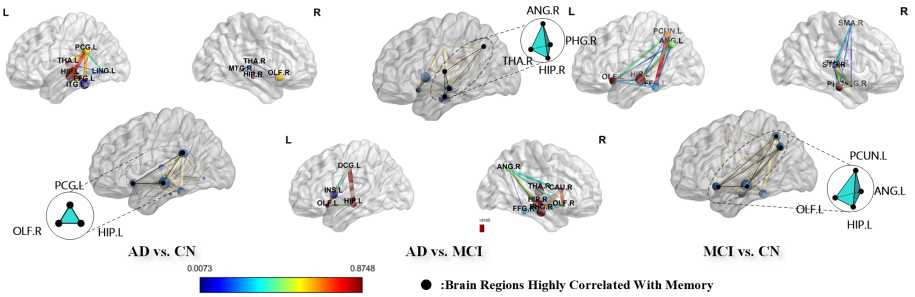

Fig. 3. Brain network analysis showing the top 10 most important regions and their connections, with a focus on memory-related regions in each task.

Memory Network Reorganization in AD: Our anatomy-guided graph learning framework identifies memory-critical hubs via multimodal topological analysis. HIP.L shows progressive disconnection in AD [28], strongly linked to episodic memory decline, with HIP.L-PHG.L connectivity predicting encoding failure [29]. Early AD sees ANG.R/PHG.R temporarily strengthen connectivity [30], buffering visual memory loss. However, the OLF.L-HIP.L pathway collapses in late AD [31], reducing global network efficiency and marking a key transition for intervention. Capturing these memory-specific network signatures [32], our model outperforms traditional biomarker-based classifiers

4 Conclusion

AD progression manifests through structural-functional interdependencies that transcend anatomical boundaries. Our multimodal graph framework overcomes existing neuroimaging limitations by preserving regional detail while modeling dynamic cross-modal interactions. Atlas-guided biomarkers combined with channel-wise feature refinement enable precise tracking of neurodegeneration in memory-critical circuits like hippocampal-entorhinal pathways. ADNI validation demonstrates superior diagnostic accuracy through biologically grounded sMRI-PET fusion, with graph topology revealing transitions from localized compensation to global network collapse. This anatomically constrained approach bridges spatial precision with connectivity dynamics, advancing computational modeling of AD progression while providing clinically interpretable biomarkers aligned with neurodegenerative trajectories.

Acknowledgement: This work was supported partly by National Natural Sci-

ence Foundation of China (Grant Nos. 62271328, 62171312 and U22A2024), National Natural Science Foundation of Guangdong Province (No. 2024A1515011950), Shenzhen Science and Technology Program (Grant Nos. JCYJ20241202124202004 and JCYJ20220818095809021), and Shenzhen Medical Research Funds (Nos. C2401023 and C2301005).

Disclosure of Interests: The authors have no competing interests to declare that are relevant to the content of this article.

References

1. Alzheimer's Association.: 2023 Alzheimer's disease facts and figures. Alzheimer's Dement, 19(4), 1598–1695 (2023)
2. Fischl, B., Dale, A. M.: Measuring the thickness of the human cerebral cortex from magnetic resonance images. Proceedings of the National Academy of Sciences, 97(20), 11050–11055 (2000)
3. Portet, F., *et al.*: Mild cognitive impairment (MCI) in medical practice: a critical review of the concept and new diagnostic procedure. Report of the MCI Working Group of the European Consortium on Alzheimer's Disease. J. Neurol., Neurosurg. Psychiatry, 77(6), 714–718 (2006)
4. Damulina, A., *et al.*: Cross-sectional and longitudinal assessment of brain iron level in Alzheimer disease using 3-T MRI. Radiology, 296(3), 619–626 (2020)
5. Park, C., Suk, H.-I.: Deep Joint Learning of Pathological Region Localization and Alzheimer's Disease Diagnosis. arXiv preprint arXiv:2108.04555 (2021)
6. Zuo, Z., *et al.*: Probabilistic MRI Brain Anatomical Atlases Based on 1,000 Chinese Subjects. PLoS ONE, 8(1), e50939 (2023)
7. Yang, Y., Mao, Y., Liu, X., Liu, X.: BrainMAE: A Region-aware Self-supervised Learning Framework for Brain Signals. arXiv preprint arXiv:2406.17086 (2024)
8. Damulina, A., *et al.*: Cross-sectional and longitudinal assessment of brain iron level in Alzheimer disease using 3-T MRI. Radiology, 296(3), 619–626 (2020)
9. Pathak, A., Menon, S. N., Sinha, S.: Mesoscopic architecture enhances communication across the Macaque connectome revealing structure-function correspondence in the brain. arXiv preprint arXiv:2007.14941 (2020)
10. Morano, J., Aresta, G., Grechenig, C., Schmidt-Erfurth, U., Bogunović, H.: Deep Multimodal Fusion of Data with Heterogeneous Dimensionality via Projective Networks. arXiv preprint arXiv:2402.01311 (2024)
11. Jack Jr, C. R., Bernstein, M. A., Fox, N. C., Thompson, P., Alexander, G., Harvey, D., Borowski, B., Britson, P. J., Whitwell, J. L., Ward, C., *et al.*: The Alzheimer's Disease Neuroimaging Initiative (ADNI): MRI methods. J Magn Reson Imaging, 27(4), 685–691 (2008)
12. Kipf, T. N., Welling, M.: Semi-supervised classification with graph convolutional networks. arXiv preprint arXiv:1609.02907 (2017)
13. Cover, T., Hart, P.: Nearest neighbor pattern classification. IEEE Transactions on Information Theory, 13(1), 21–27 (1967)
14. Tzourio-Mazoyer, N., Landeau, B., Papathanassiou, D., Crivello, F., Etard, O., Delcroix, N., Mazoyer, B., Joliot, M.: Automated anatomical labeling of activations in SPM using a macroscopic anatomical parcellation of the MNI MRI single-subject brain. Neuroimage, 15(1), 273–289 (2002)

15. Tran, D., Wang, H., Torresani, L., Feiszli, M.: Design light-weight 3D convolutional networks for video recognition: Temporal residual, fully separable block, and fast algorithm. arXiv preprint arXiv:1905.13388 (2019)
16. Zhao, L., Akoglu, L., Matta, V., Akoglu, E.: A Comprehensive Survey on Dynamic Graph Neural Networks. arXiv preprint arXiv:2006.00116 (2020)
17. Tran, D., Wang, H., Torresani, L., Ray, J., LeCun, Y., Paluri, M.: A closer look at spatiotemporal convolutions for action recognition. In: Proceedings of the IEEE Conference on Computer Vision and Pattern Recognition, pp. 6450–6459 (2018)
18. Song, H., Wang, R., Gen, K., Li, Z., Wang, Y.: Spatio-temporal attention-based LSTM networks for traffic flow forecasting. In: Proceedings of the AAAI Conference on Artificial Intelligence, vol. 32, no. 1 (2018)
19. Hu, J., Shen, L., Albanie, S., Sun, G., Wu, E.: Squeeze-and-Excitation Networks. arXiv preprint arXiv:1709.01507 (2017)
20. Ziegler, G., Dahnke, R., Jäncke, L., Yotter, R. A., May, A., Gaser, C.: Cortical thinning in healthy aging: Investigating patterns and possible confounders. Neurobiology of Aging, 34(1), 1–12 (2013)
21. Buckner, R. L.: Hipppocampal-cortical memory networks and Alzheimer's disease. Neuron, 46(4), 625–628 (2005)
22. Seeley, W. W., Crawford, R. K., Zhou, J., Miller, B. L., Greicius, M. D.: Neurodegenerative diseases target large-scale human brain networks. Neuron, 62(1), 42–52 (2009)
23. Frisoni, G. B., Fox, N. C., Jack Jr, C. R., Scheltens, P., Thompson, P. M.: The clinical use of structural MRI in Alzheimer disease. Nature Reviews Neurology, 6(2), 67–77 (2010)
24. Tosun, D., Landau, S., Aisen, P. S., Petersen, R. C., Mintun, M., Weiner, M. W.: Imaging-based diagnostic approaches for Alzheimer's disease: Progress and prospects. Alzheimer's Dementia, 12(2), 225–235 (2016)
25. Raj, A., Kuceyeski, A., Weiner, M.: A network diffusion model of disease progression in dementia. Neuron, 73(6), 1204–1215 (2012)
26. Salas-Gonzalez, D., Toussaint, P. J., Fontanella, S., Maréchal, B., Routier, A., Coupe, P.: Connectome-based propagation model in Alzheimer's disease. Medical Image Analysis, 60, 101618 (2020)
27. Seeley, W. W., Crawford, R. K., Zhou, J., Miller, B. L., Greicius, M. D.: Neurodegenerative diseases target large-scale human brain networks. Neuron, 62(1), 42–52 (2009)
28. Raj, A., Kuceyeski, A., Weiner, M.: A network diffusion model of disease progression in dementia. Neuron, 73(6), 1204–1215 (2012)
29. Yassa, M. A., Stark, S. M., Bakker, A., Albert, M. S., Gallagher, M., Stark, C. E.: High-resolution structural and functional MRI of hippocampal CA3 and dentate gyrus in patients with amnestic mild cognitive impairment. NeuroImage, 51(3), 1242–1252 (2011)
30. Jones, D. T., Graff-Radford, J., Lowe, V. J., Wiste, H. J., Gunter, J. L., Senjem, M. L., Botha, H., Kantarci, K., Boeve, B. F., Knopman, D. S., Petersen, R. C., Jack Jr, C. R.: Adaptive basal ganglia network connectivity in preclinical Alzheimer's disease. Brain, 139(10), 2837–2850 (2016)
31. Khan, W., Kanel, P., Zhang, W., Ofori, E., Okonkwo, O., Blennow, K., Zetterberg, H., Sporns, O., Gold, B. T.: Olfactory network degeneration in early-stage Alzheimer's disease. NeuroImage, 218, 116977 (2020)
32. Mesulam, M. M.: From sensation to cognition. Brain, 121(6), 1013–1052 (1998)